IEEE Access
Multidisciplinary | Rapid Review | Open Access Journal

Received September 5, 2019, accepted September 17, 2019, date of publication September 23, 2019,
date of current version October 9, 2019.

Digital Object Identifier 10.1109/ACCESS.2019.2942959

Optimized Autofluorescence Spectral Signature for Non-Invasive Diagnostics of Ocular Surface Squamous Neoplasia (OSSN)

ABBAS HABIBALAHI[1,5,6], ALEXANDRA ALLENDE[2,3], CHANDRA BALA[4], AYAD G. ANWER[1,6], SUBHAS MUKHOPADHYAY[5], (Fellow, IEEE), AND EWA M. GOLDYS[1,6]

[1]ARC Centre of Excellence Centre for Nanoscale BioPhotonics, University of New South Wales, Sydney, NSW 2032, Australia
[2]Douglass Hanly Moir Pathology, Macquarie Park, Sydney, NSW 2113, Australia
[3]Faculty of Medicine and Health Sciences, Macquarie University, Sydney, NSW 2109, Australia
[4]Department of Ophthalmology, Faculty of Medicine and Health Sciences, Macquarie University, Sydney, NSW 2109, Australia
[5]School of Engineering, Macquarie University, Sydney, NSW 2109, Australia
[6]Graduate School of Biomedical Engineering, University of New South Wales, Sydney, NSW 2032, Australia

Corresponding author: Abbas Habibalahi (a.habibalahi@unsw.edu.au)

This work was supported in part by the Personal Eyes Pty Ltd under Grant 5201600708, in part by the ARC Centre of Excellence for Nanoscale Biophotonics under Grant CE140100003, and in part by the iMQRES Scholarship.

ABSTRACT Clinical OSSN diagnostics by non-invasive spectral imaging of eye autofluorescence must be rapid enough to be comfortable for patients – without compromising accuracy. This requires identifying optimized spectral signatures of OSSN based on a minimal number of spectrally defined images. Here, we identified such signatures using a data-driven methodology of swarm intelligence. Ten patients with histopathological diagnosis of ocular surface squamous neoplasia (OSSN) were recruited. Their unstained biopsy OSSN specimens were investigated using a custom-built autofluorescence multispectral microscopy imaging system. The images were taken in 38 spectral channels spanning specific excitation (340 nm-510 nm) and emission (420 nm-650 nm) wavelength ranges. To identify optimized spectral signatures of OSSN from a small number of channels, swarm intelligence was combined with discriminative cluster analysis. This study established an optimized spectral signature of OSSN derived from multispectral data taken in 38 channels. Depending on the critical nature of the application and the consequences of misclassification error, two optimized spectral signatures with 5 and 10 channels were obtained which reduced the imaging time to 20 and 40 seconds, a reduction by 75% and 80 %, respectively. The K-nearest neighbor classifier was then built using OSSN spectral signatures and optimized to successfully detect OSSN with $\sim$1% and $\sim$14% misclassification error using 10 and 5 channels, respectively. Our study found an optimized spectral signature of OSSN allowing rapid diagnostic imaging in clinical settings and demonstrates the feasibility of using optimized multispectral autofluorescence spectral signatures to detect and determine boundaries of OSSN.

INDEX TERMS Ocular surface squamous neoplasia (OSSN), autofluorescence spectral signature, swarm intelligence.

I. INTRODUCTION

Ocular surface squamous neoplasia (OSSN) is a broad term encompassing premalignant and malignant changes of the corneal and conjunctival epithelium [1], [2]. OSSN includes mild, moderate and severe dysplasia, squamous cell carcinoma in situ and invasive squamous cell carcinoma, reflecting the progression of severity of neoplasia from mild dysplasia at one end of the spectrum to invasive carcinoma at the opposite end [3]–[5]. Currently the gold standard for diagnosis and further management of OSSN relies on invasive histological examination [6], which induces patient trauma [2] and causes scarring and potentially limbal stem cell deficiency in patients [7], [8]. Histology analysis of tissue biopsies requires processing, sectioning, and staining of specimen, which is time and labor intensive [9]. This method is subject to processing issues such as tangential sectioning and fragmentation which can hamper interpretation of margin

The associate editor coordinating the review of this manuscript and approving it for publication was Wei Liu.

clearance [7], [8], [10]. Also difficulties exist in excising subtle lesions with ill-defined margins, which may result in incompletely excised lesions or removing excessive non-neoplastic tissue [11]. Impression cytology is also used to detect OSSN which is a less invasive OSSN diagnostic method compared to tissue biopsy [12], [13]. However, this technique is operator dependent and limited to superficial sampling of cells so that invasive carcinoma cannot be reliably identified [14], [15]. In vivo confocal microscopy (IVCM) [16] and anterior segment optical coherence tomography (OCT) [17] are non-invasive imaging modalities that have shown mixed results when findings are correlated with tissue biopsies with operator dependent limitations and limited capability in assessing thick keratotic lesions or superficially invasive carcinomas [18].

Our group has recently introduced autofluorescence multispectral imaging (AFMI) as a potential replacement for OSSN biopsy in the future [11]. AFMI offers distinctive benefits for the detection of OSSN as it is contactless, non-invasive, free of staining and contrast agents and can produce real-time results in an outpatient setting [11]. AFMI-based diagnostics of OSSN is possible because the OSSN cells are characterized by their specific spectral signature which AFMI is able to capture [11]. These spectral signatures capture cancer-induced variations in chemical composition of tissue [19]. Metabolic transformations in cancer are reflected in naturally fluorescent compounds present in cells and tissues such as protoporphyrin IX (PPIX), reduced nicotinamide adenine dinucleotide (NADH) and flavin adenine dinucleotide (FAD) [20]–[23]. AFMI scans autofluorescence light produced by eye tissue cells during excitation, by safe levels of artificial light; this scanning is carried out in a number of spectral channels which allows capturing the autofluorescent spectral signatures of OSSN [11].

The AFMI technology is very flexible regarding the number of employed channels and their associated excitation and emission wavelength ranges, which is an improvement over the current standard ophthalmological autofluorescence imaging where patients' images are typically taken without any spectral selection [24], [25]. The spectral selection in the AFMI technology has the potential to be incorporated into a standard retinal camera setup for a regular eye examination to confirm OSSN at the clinic using a simple eye scan, so that appropriate action can be quickly taken by a specialist [16], [26]. It has been previously reported that the OSSN spectral signature can be identified using a large number of spectral channels (Nch = 38) [11]. However, tens of spectral channels used in [11] represent a translational barrier making AFMI diagnostics inconvenient for patients. Imaging in each spectral channel at the maximum eye-safe excitation limit requires several second camera exposure to improve spectral image signal to noise ratio by increasing the amount of autofluorescence light which reaches the camera sensor [27]. As a result, employing tens of channels leads to prolonged imaging time, during which unintentional eye movement and blinking may cause unavoidable interference such as image shifts and defocusing [28]. Therefore, to enable clinical translation of AFMI and its deployment for ophthalmologic applications, a robust methodology must be developed to identify the smallest number of imaging channels with optimized spectral specifications which can accurately determine the spectral signature of OSSN. In addition, such an optimized OSSN signature can also be referred as OSSN spectral biomarker which has the potential to assist the clinical practice in learning disease-specific patterns and their interactions [29]. Investigating such a signature reveals which fluorophores vary in tissue when OSSN occurs [19]. Correlating such signature with OSSN may give an understanding of the underlying processes that produced the data.

Establishing an optimized OSSN spectral signature can be undertaken by means of traditional methods such as selecting a minimal number of channels by a previously identified features regarded as a specific ''biomarker'' (for example the content of PPIX as a cancer biomarker [22]) is a suboptimal way of identifying an optimized OSSN spectral signature [30]. This approach is restricted only to the features associated with a known biomarker, and it does not permit to find the unknown and potentially more informative features that were not part of the channels associated with the known biomarkers. Scoring the intrinsic properties of each channel by applying statistical tests such as weighting factors [31], [32] is a feasible but inefficient approach to identify a precise OSSN spectral signature from a small number of channels [33]. Grouping the channels that are individually significant for OSSN identification does not necessarily result in an efficient classification performance due to the potential for information overlap between channels with close spectral specifications [34]–[36]. Therefore, to select an optimal subset of channels capturing OSSN signature effectively, mutual interactions between channels need to be considered [37], and the usefulness of each channel is evaluated simultaneously with other channels.

In this study, we report the optimized OSSN spectral signature. To this end, we advance traditional band selection analysis and present an artificial intelligence method to find the spectral signature of OSSN based on an optimized number of spectral channels and spectral specifications. The optimization strategy in this study had two phases: (i) search for a subset of channels adequately representing the OSSN spectral signature and (ii) quality evaluation of channel subsets. In order to search for such subset of channels, we used swarm intelligence, a method that draws on collective behavior of a group of naïve agents [38], [39]. We then employed a criterion function to evaluate the quality of the channel subset proposed by swarm intelligence [40]–[42]. To this end, OSSN and normal (non-neoplastic) clusters were formed through discrimination analysis [43] based on the channels suggested by swarm intelligence [44], and then a standard criterion function was defined to evaluate the quality of clusters as a selection measure. Our criterion function is

defined based on the separation distance of the normal (non-neoplastic) and OSSN cluster, and it can take arbitrary values (so it is boundless). Maximizing such a criterion function leads to a superior optimization of the OSSN spectral signature. Conversely, the feature selection methods using a classifier such as support vector machine (SVM) [45] are limited by the saturation of the performance curve (ROC) saturation (AUC = 1) [46]. This saturation occurs at a point when the non-neoplastic and neoplastic clusters just become completely separated [47]. Our method is able to continue maximizing the separation of non-neoplastic and neoplastic clusters even if they no longer overlap and are far away from each other. This provides a superior OSSN spectral signature compared to what could be obtained by feature selection with classifiers. To minimize the influence of confounders such as eye color and/or various amounts of sunlight exposure, which are known factors related to incidence and development of OSSN, and which can interfere with identification of the optimized OSSN spectral signature, the criterion function reflecting the neoplastic signature is calculated on the intra-patient basis and then averaged over available patients. Such methodology [48] combines the advantage of both inter-patient and intra-patient frameworks [49] and largely protects the band selection strategy from inter-patient variability related to patient factors. In order to evaluate the generalization of the methodology, two levels of cross-validation were employed during channel selection processes. The generality power of the proposed method was evaluated blindly on the data derived from testing patients which did not have any contribution to developing the model. This approach avoids potential overfitting. Using the methodology proposed in this study, we were able to successfully discover an optimized OSSN spectral signature.

II. METHOD

A. SAMPLE COLLECTION AND THE GOLD STANDARD

Ten patients with positive OSSN diagnosis were recruited under permission from Macquarie University Human Research Ethics Committee, reference No: 5201600708. Written consent forms were obtained from participants after explanation of the nature of the potential consequences of this research. This study also fully followed tents of the Declaration of Helsinki. We collaborated with Douglass Hanly Moir Pathology to collect fixed tissue sections. For each patient, a pair of adjacent sections were investigated which were formalin-fixed, dehydrated, paraffin-embedded and dewaxed. Further, one haematoxylin and eosin (H&E) stained section was used as our reference, and another section was cover-slipped without staining and used for our multispectral analysis. In this way we were able to identify regions of interest (ROI) on the H&E section and then identify a corresponding region on the matched unstained section. Traditional histological features based on cytological atypia such as disordered maturation, pleomorphism, and degree of epithelial involvement were used to categorize lesions as non-neoplastic or neoplastic [50], [51] on the H&E stained slides.

TABLE 1. Spectral channels used in this study.

ChNo	Excitation Wavelength (nm)	Emission Wavelength (nm)
1	340±5	420-460
2	368±5	420-460
3	373±5	420-460
4	378±5	420-460
5	382±5	420-460
6	388±5	420-460
7	340±5	454-495
8	368±5	454-495
9	373±5	454-495
10	378±5	454-495
11	382±5	454-495
12	388±5	454-495
13	391±5	454-495
14	*394*±5	454-495
15	*405*±5	454-495
16	340±5	573-613
17	*368*±5	573-613
18	*373*±5	573-613
19	*378*±5	573-613
20	*382*±5	573-613
21	*388*±5	573-613
22	*391*±5	573-613
23	*394*±5	573-613
24	*405*±5	573-613
25	*413*±5	573-613
26	432±5	573-613
27	441±5	573-613
28	455±5	573-613
29	460±5	573-613
30	470±5	573-613
31	491±5	573-613
32	510±5	573-613
33	382±5	575-650
34	388±5	575-650
35	391±5	575-650
36	394±5	575-650
37	405±5	575-650
38	413±5	575-650

To this end, lesions with various grades of dysplasia (mild, moderate, severe) and SCCIS or SCC were characterized as OSSN, and other regions were identified as non-neoplastic [11]. Both non-neoplastic and OSSN areas were available for each patient, yielding a total of 10 samples from 10 eyes (7 right, 3 left) of 10 patients (40 to 82 years old) for multispectral analysis.

B. IMAGE ACQUISITION AND DATA GENERATION

A full description of the multispectral system used in this study is given in [11]. Briefly, the system is an adapted IX83 Olympus microscope [11] equipped with 18 narrow-band excitation wavelengths (±5nm) provided by low power LEDs and 4 filter cubes to produce defined spectral regions, spanning broad excitation (340 nm-510 nm) and emission (420 nm-650 nm) wavelength ranges. Each pair of excitation/emission wavelength regions defined using a filter cube creates a distinctive spectral channel, and we employed 38 of such channels (Table.1) to generate a sequence of fluorescence images of the same sample area containing different spectral information. The spectral images were taken from the unstained tissue at 40 times magnification (40x). Further, the spectral images were pre-processed to remove the uninformative background, non-uniform illumination of the field of view and random noises [43], [52] as reported in [11]. To generate specific quantitative spectral information, the spectral images were divided into non-overlapping sectors (square of 10 x10) which covered the whole ROI for each sample. Further, fluorescence intensity was averaged over each sector in each channel, to produce a vector with 38 elements corresponding to the number of the channels (Nch = 38). This vector is referred to as the spectral signature of that sector, and it was assigned a label as non-neoplastic or neoplastic depending on the pathological assessment of the area where the sector was extracted. These sample tissue sectors are referred to as datapoints in this study.

C. DATA ANALYSIS

FIGURE 1 demonstrates the data analysis methodology employed in this study to discover the optimized OSSN spectral signature. To ensure external cross-validation [53], the patients were randomly split into two groups: ''model generating'' patients and ''validating'' patients [54]. The ''model generating patients'' group consisted of 70% of patients (N = 7) which were used to develop the algorithm and the remaining 30% of patients (N = 3) were put aside for our later blind validation of model fidelity of new patients.

Further, the ''model-generating'' patients were employed to develop the optimization model which combined discriminative cluster analysis discovering OSSN and non-neoplastic clusters and swarm intelligence. This model iterated between the step of swarm intelligence search for a subset of channels adequately representing OSSN signature [11] and the step of providing feedback found by discriminative cluster analysis about the OSSN and non-neoplastic clusters separation power, which can be referred to the robustness of the OSSN spectral signature. This back and forth iteration between swarm intelligence and discriminative cluster analysis continued until the algorithm achieved convergence and no further improvement in the robustness of the OSSN spectral signature could be identified. To avoid constructing an inefficient model corresponding too closely to the training data points and therefore fail to deal with unseen datapoints reliably, internal cross-validation was also employed. To achieve this aim, the data points obtained from each patient used for developing the model were divided into two sets: the training data set, comprising 60% of data points of the patient under consideration were used to establish the OSSN spectral signature and the testing data set, comprising the remaining 40% of data points of the same patient was used to evaluate the robustness of the proposed OSSN spectral signature and which was then fed back to the swarm intelligence algorithms.

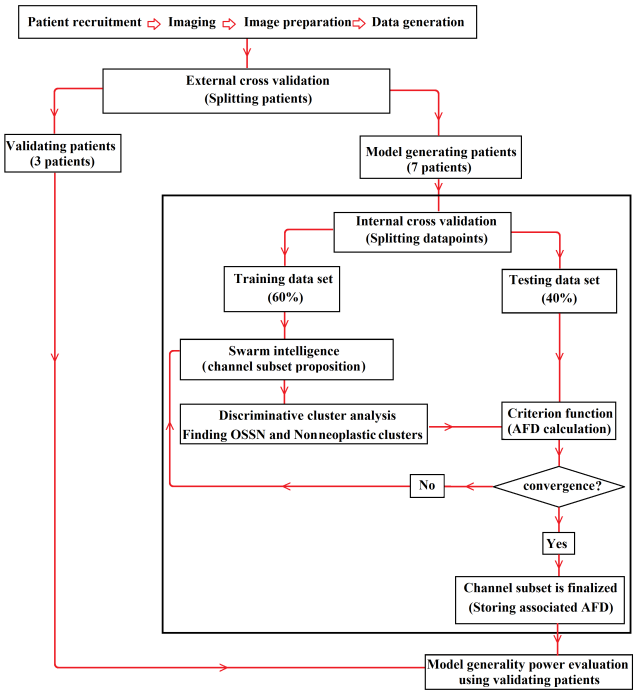

FIGURE 1. Methodology for optimized OSSN spectral signature discovery.

D. DISCRIMINATIVE CLUSTER ANALYSIS AND CRITERION FUNCTION

In this study, discriminative cluster analysis [55] was used to find OSSN and non-neoplastic data clusters using the nominated channels; which were then used to evaluate the strength of OSSN-specific spectral signature. The non-neoplastic and OSSN clusters were found using a 2-D discriminative space spanned by two canonical variables [44]; these are optimal linear combinations of the proposed channels yielding the spectral signature which ensures the best separation of non-neoplastic and OSSN clusters. This signature can also be colloquially referred to as ''color'' because, just like colour, it represents a linear mixture of light signals at different wavelengths.

Further, the testing data sets were projected onto the discriminative space generated to establish how well the non-neoplastic and OSSN data clusters are separated. A quantitative criterion function was defined to measure the strength of the OSSN spectral signature which is dependent on the selection of channels. This criterion function is based on determining Fisher distance (FD) [56]; the ratio of between-cluster and within-cluster variances. The FD was

calculated using the testing points obtained from internal cross-validation which did not contribute to the development of the discriminative space. To minimize the interference of interpatient confounders such as different exposure to sunlight etc., the FD was calculated for each patient separately and then averaged over all patients available in the training cohort. This strategy enhances the channel selection process to more accurately detect neoplastic changes, as confounders are considered to affect the tissue sections equally when they are obtained from the same patient. Therefore, the Averaged Fisher distance (AFD) was used as our criterion function to measure the discrimination power of the spectral signature.

E. DISCRIMINATIVE CLUSTER ANALYSIS AND CRITERION FUNCTION

Swarm intelligence is inspired by the evolution of a group of simple information-processing interacting agents [57]. In this approach, the naive artificial agents cooperate via low-level communication to find the OSSN signature as a complex optimization problem. First, they generate a population of the agents and assess the associated criterion function, and then repeatedly update the agents via a specific evolutionary strategy until the convergence condition is satisfied. In this study, we chose the agents to be candidate channel subsets of all available channels (Nch = 38), while the AFD served as the criterion function. These agents have different behavior to optimize the search study depending on their evolutionary strategies. To find the most efficient evolutionary strategy which can effectively identify a group of the best channels providing the OSSN spectral signature, we tested three evolution strategies including ant colony optimization (ACO) [58], [59], particle swarm intelligence (PSO) [60]–[62] and differential evaluation (DE) [63].

III. RESULTS AND DISCUSSION

Optimizing the OSSN spectral signature is a multiple (two) objective optimization problem [64] as we need to minimize the number of the employed channels, and also find the best spectral specifications of these channels. We simplified this two-objective optimization problem into two one-objective optimization problems: (i) optimizing the spectral signature content which aims to define the spectral specification of the OSSN signature, and, (ii) optimizing the channel number of the OSSN signature (K).

A. OPTIMIZING THE OSSN SPECTRAL SIGNATURE CONTENT

First, the spectral signature channel number was set to K = 2, and an optimized channel subset with associated AFD value was found and recorded. The same optimization methodology was repeated 29 times while the spectral signature channel number (K) was increased by one at a time to identify the optimized OSSN spectral signature with different channel numbers, from (k = 2 to k = 30). As an example, detailed results of optimizing the OSSN spectral signature content using 6 channels ($N_{ch} = 6$) are presented here. After applying

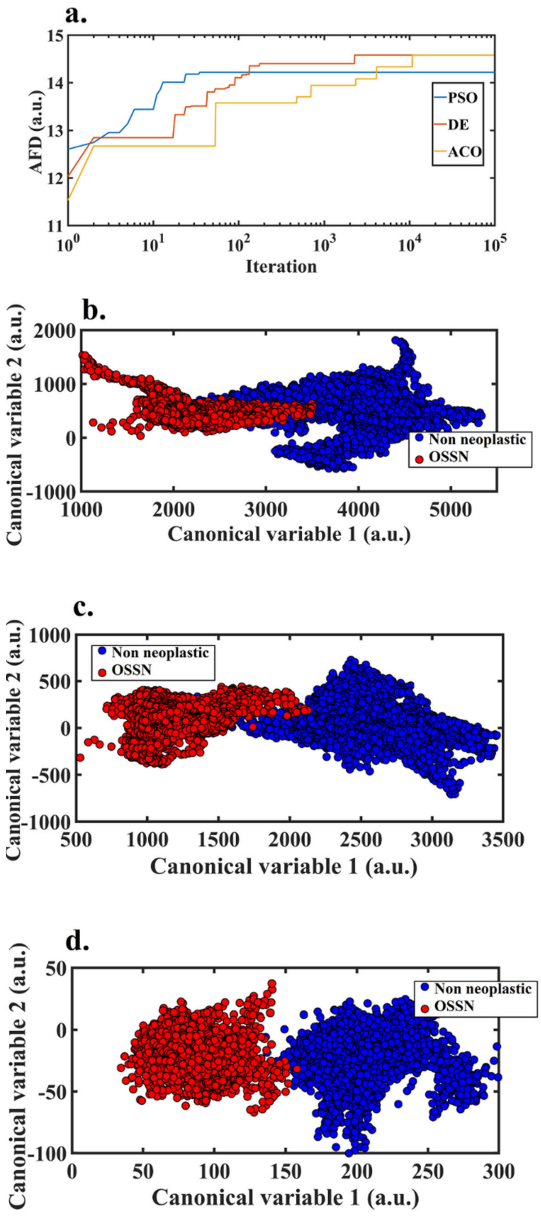

FIGURE 2. (a) AFD vs. number of iterations using PSO, ACO, DE. Cluster improvement due to selecting more effective channel subsets using ACO: (b) after 10 iterations, (c) after 100 iterations, (d) after 105 iterations and achieving satisfactory convergence of the algorithm.

the external cross validation, internal cross-validation was performed in the process of the developing model, and data points were divided into training (60%) and testing (40%) data for each patient. Then, the ACO, DE and PSO algorithms with 50 agents were executed, using 10^5 iterations ($m_i = 10^5$), where each iteration selected 6 channels of the total 38 channels. For each run, the discrimination space was generated using the training data, and the AFD was calculated using the testing data.

Figure 2(a) represents the performance of PSO, ANT and DE algorithms used to optimize AFD in 105 iterations, which shows that all three algorithms converged before 104 iterations, after which that no appreciable variation in the criterion

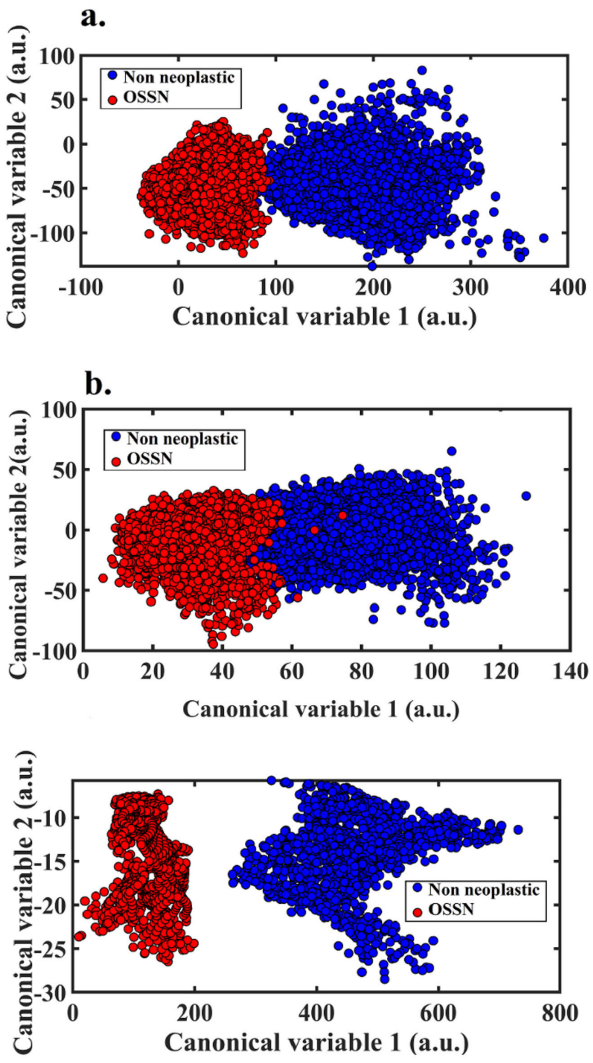

FIGURE 3. Validating optimized OSSN spectral signature (Nch = 6) on three test patients put aside from external cross-validation. (a-c) Non-neoplastic and OSSN clusters of three validating patients found by optimized spectral signature with 6 channels proposed by DE.

function could be observed. Both DE and ANC reached a higher AFD (AFD = 14.58) compared to PSO (AFD = 14.22), and DE was the fastest algorithm to converge (mi <2500). Figure 2 (b-e) show increasing separation of the OSSN and non-neoplastic clusters as the number of iterations increased from mi = 10 to mi = 105 as the criterion function continued to be optimized. The generalization power of the optimized spectral signature (Nch = 6) was evaluated on validated patients which were put aside from external cross-validation, that means data from patients who did not have any contribution to developing the model of optimized OSSN spectral signature. The validation data points were generated and projected onto the discriminative space generated by 6 optimized channels. Figure 3 (a-c) show that the optimized OSSN spectral signature could successfully separate the OSSN cluster of sectors from the non-neoplastic cluster in all 3 patients, which demonstrates the generalization capability of the methodology proposed in this study.

TABLE 2. Optimizes OSSN spectral signatures.

Signature ID	Signature channel number	Scanning time	Evolutionary strategy	Employed channels
SID 1	3	~12 sec	DE	CH2- CH5- CH34
SID 2	5	~20 sec	DE	CH3- CH5- CH16- CH34- CH37
SID 3	10	~40 sec	DE	CH1- CH2- CH6- CH11- CH16- CH19- CH21- CH24- CH34- CH37
SID4	38	~150 sec	Not applicable	All channels

B. OPTIMIZING OSSN SPECTRAL SIGNATURE CHANNEL NUMBER

Having optimized the spectral content of OSSN signature with different channel numbers, we determined the AFD as a function of the spectral signature channel number using ACO, PSO, and DE. Figure 4 (a) shows that DE had a slightly better performance to maximize AFD and, therefore, it is identified as our best evolutionary swarm intelligence algorithm in this study. Figure 4 (a) also demonstrates that the discriminative performance (AFD) steadily increases with increasing number of spectral channels (Nch) used for the OSSN spectral signature. However, it can be observed that the AFD improvement rate as a function of the number of channels substantially decreases with increasing Nch. To quantify the improvement rate of the OSSN signature against channel number, the corresponding derivative function of AFD corresponding to DE is shown in Figure 4 (b). This plot shows the improvement rate decreases significantly for Nch = 5 (rate ~1) and there is a negligible AFD improvement (close to zero) when the number of channels used to determine the OSSN spectral signature increases beyond Nch = 10.

To demonstrate the performance of the optimized OSSN spectral signature determined by swarm intelligence to detect and delineate OSSN, a K nearest neighbor (KNN) classifier [65] was developed in an intra-patient framework, as reported in [11]. In this framework, the KNN classifier was trained based on a single patient and then tested on another part of the tissue from the same patient (testing area). Three optimum spectral signatures which used 3, 5 and 10 channels (Table 2) were selected, and their performances were evaluated against the OSSN spectral signature formed by all channels (Nch = 38). After training the KNN classifiers using spectral signatures (SID1-4) obtained from the unstained tissue, the trained classifiers were then applied to the sectors of the testing area of the same patient which were not used to form the classifier for the label prediction (''neoplastic'' vs ''non-neoplastic'').

To generate the false-color map of these sections (Figure 4 (e-l)), the extracted sectors were colored in red or green depending if they were, respectively, predicted to be OSSN or non-neoplastic by the associated classifier. As a reference, Figure 4 (c) and (d) also shows the histology assessment of the non-neoplastic and OSSN regions with red and

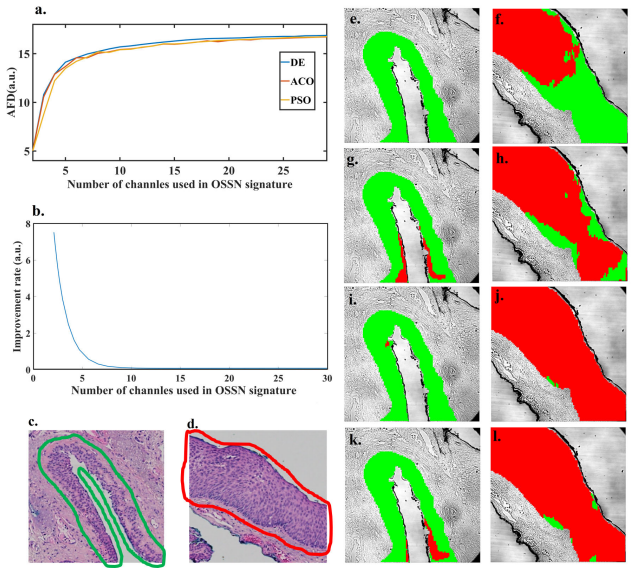

FIGURE 4. **(a) ACO, PSO, and DE performance to optimize OSSN spectral signature with respect to the channel number of the spectral signature. (b) improvement rate of OSSN discriminative power as a function of spectral signature channel number. (c) and (d) H&E analysis of non-neoplastic and OSSN outlined by green and red lines, respectively, of an example testing patient. (e),(f) False color map of non-neoplastic and OSSN section, respectively predicted by KNN classifier trained by SID1. (g),(h) False color map of non-neoplastic and OSSN section, respectively predicted by KNN classifier trained by SID2. (i),(j) False color map of non-neoplastic and OSSN section, respectively predicted by KNN classifier trained by SID3. (k), (l) False color map of non-neoplastic and OSSN section, respectively predicted by KNN classifier trained by SID4.**

green dashed line representing the boundary of OSSN and non-neoplastic areas, respectively. Figure 4 (e-f) / Figure 4 (g-h) / Figure 4 (i -j)/ Figure 4 (k-l) show the corresponding false color maps which were predicted by the KNN classifier trained by the SID1/SID2/SID3/SID4 OSSN spectral signatures.

Figure 4 (e-l) demonstrate that the best accuracy was obtained from an optimal OSSN spectral signature with 10 channels ($<$1% misclassification errors) in both non-neoplastic and OSSN sections. Employing 5 channels led to $\sim$15% and $\sim$ 13% misclassification error in the OSSN and non-neoplastic sections, respectively. Figure 4 (e) and (f) demonstrate that using SID1 employing 3 channels led to a practically nil misclassified error in the non-neoplastic section; however, a high misclassification error ($\sim$46%) in the OSSN section. Figure 4 (k) and (l) shows that 2% and 10% misclassification error was present for the OSSN and non-neoplastic section, respectively when the KNN classifier was trained using SID4. This means that SID4 which employed all channels (Nch = 38) led to a higher misclassification error than when SID3 employing Nch = 10 channels was used. We attribute this difference to the detrimental contribution of irrelevant channels in the spectral signature. Each additional channel feeds the classifier with discriminative information along with some unavoidable interference. Although our image preparation minimized some corrupting sources of interference (see section II.B), their full effect cannot be completely removed. Therefore, irrelevant or highly correlated channels which have no discriminative information feed the classifier only with corrupting interference, which negatively affects the results.

A decision on the number of required channels depends on various factors including the limitation of scanning time, the criticality of the application and equipment limitations. Although the spectral signature from 5 channels (or even 3 channels) could not reliably delineate the boundary of OSSN, it can be sufficiently accurate for a routine eye scan in doctor's office and support physicians in their initial decision making. A few numbers of the channels to detect OSSN can significantly reduce the scanning time, especially for the large size lesions where physicians need to examine several points of the lesion. If the AFMI is intended for accurate boundary detection in the operating room, or for monitoring OSSN over the treatment period such as chemotherapy or possible recurrence, employing 10 channels would be recommended. However, employing more than 10 channels appears counterproductive as irrelevant channels not only increase the scanning time (38 channels scanning time $\sim$ 150 s) and instrumentation cost but also reduce the performance of the classifier. Using 5 channels for simple scanning and 10 channels for the critical applications reduce the scanning time by 87% (scanning time $\sim$ 20 s) and 73% (scanning time $\sim$ 40 s), respectively, which translates to more patient-friendly AFMI technology in a real ophthalmology setting.

IV. CONCLUSION

The recently introduced AFMI opens the opportunity of spectral imaging employing a large number of spectral channels with defined excitation and emission wavelength ranges. This makes it possible to extract spectral signatures for OSSN. However, in clinical ophthalmic applications such as diagnosis of OSSN or identification of cancer boundaries, such signature needs to be optimized in terms of spectral content and the number of channels. These reduce the imaging time without sacrificing classification accuracy. This study identified a richly informative spectral signature able to rapidly differentiate normal (non-neoplastic) and diseased (OSSN) tissue through a combination of cluster analysis and swarm intelligence. Identifying the optimized spectral signature of OSSN was formulated in this work as a two-objective optimization task with a fitness function reflecting the discriminative performance of the spectral signature and the reduction in the number of elements. Three swarm intelligence methods including PSO, DE, and ACO well established in the domain of machine learning were assessed, and DE was found to have the best capability to search and optimize the OSSN spectral signature. Depending on the criticality of the application, this study found spectral signatures based on 5 and 10 channels which could successfully detect OSSN while reducing the scanning time by 87% and 73%, respectively, compared to all 38 channels.

REFERENCES

[1] G. A. Lee and L. W. Hirst, "Ocular surface squamous neoplasia," *Surv. Ophthalmol.*, vol. 39, no. 6, pp. 429–450, 1995.

[2] A. Radhakrishnan, "Squamous neoplasia [OSSN]—A brief review," *Kerala J. Ophthalmol.*, vol. 23, no. 4, Dec. 2011.

[3] S. Gichuhi, M. S. Sagoo, H. A. Weiss, and M. J. Burton, "Epidemiology of ocular surface squamous neoplasia in Africa," *Tropical Med. Int. Health*, vol. 18, no. 12, pp. 1424–1443, 2013.

[4] Y. Xu, Z. Zhou, Y. Xu, M. Wang, F. Liu, H. Qu, and J. Hong, "The clinical value of *in vivo* confocal microscopy for diagnosis of ocular surface squamous neoplasia," *Eye*, vol. 26, no. 6, p. 781–787, 2012.

[5] L. W. Hirst, R. A. Axelsen, and I. Schwab, "Pterygium and associated ocular surface squamous neoplasia," *Arch. Ophthalmol.*, vol. 127, no. 1, pp. 31–32, 2009.

[6] E. C. Pola, R. Masanganise, and S. Rusakaniko, "The trend of ocular surface squamous neoplasia among ocular surface tumour biopsies submitted for histology from Sekuru Kaguvi Eye unit, Harare between 1996 and 2000," *Central Afr. J. Med.*, vol. 49, nos. 1–2, pp. 1–4, 2003.

[7] K. Shyamala and K. H. C. Girish, and S. Murgod, "Risk of tumor cell seeding through biopsy and aspiration cytology," *J. Int. Soc. Preventive Community Dentistry*, vol. 4, no. 1, pp. 5–11, 2014.

[8] A. Galor, C. L. Karp, P. Oellers, A. A. Kao, A. Abdelaziz, W. Feuer, and S. R. Dubovy, "Predictors of ocular surface squamous neoplasia recurrence after Excisional surgery," *Ophthalmology*, vol. 119, no. 10, pp. 1974–1981, 2012.

[9] L. He, L. R. Long, S. Antani, and G. R. Thoma, "Histology image analysis for carcinoma detection and grading," *Comput. Methods Programs Biomed.*, vol. 107, no. 3, pp. 538–556, 2012.

[10] S. Gichuhi, E. Macharia, J. Kabiru, Alain M'B. Zindamoyen, H. Rono, E. Ollando, L. Wanyonyi, J. Wachira, R. Munene, T. Onyuma, M. S. Sagoo, H. A. Weiss, and M. J. Burton, "Clinical presentation of ocular surface squamous neoplasia in kenya," *JAMA ophthalmol.*, vol. 133, no. 11, pp. 1305–1313, 2015.

[11] A. Habibalahi, C. Bala, A. Allende, A. G. Anwer, and E. M. Goldys, "Novel automated non invasive detection of ocular surface squamous neoplasia using multispectral autofluorescence imaging," *Ocular Surf.*, vol. 17, no. 3, pp. 540–550, Jul. 2019.

[12] J. N. Barros, M. S. Lowen, P. L. Ballalai, V. L. D. Mascaro, J. Á. P. Gomes, and M. C. Martins, "Predictive index to differentiate invasive squamous cell carcinoma from preinvasive ocular surface lesions by impression cytology," *Brit. J. Ophthalmol.*, vol. 93, no. 2, pp. 209–214, 2009.

[13] R. Singh, A. Joseph, T. Umapathy, N. L. Tint, and H. S. Dua, "Impression cytology of the ocular surface," *Brit. J. Ophthalmol.*, vol. 89, no. 12, pp. 1655–1659, 2005.

[14] N. Tananuvat, N. Lertprasertsuk, P. Mahanupap, P. Noppanakeepong, "Role of impression cytology in diagnosis of ocular surface neoplasia," *Cornea*, vol. 27, no. 3, pp. 269–274, 2008.

[15] M. Calonge, Y. Diebold, V. Sáez, A. E. de Salamanca, C. García-Vázquez, R. M. Corrales, and J. M. Herreras, "Impression cytology of the ocular surface: A review," *Exp. Eye Res.*, vol. 78, no. 3, pp. 457–472, 2004.

[16] M. Zarei-Ghanavati, E. Mousavi, A. Nabavi, G. Latifi, H. Z. Mehrjardi, M. Mohebbi, H. Ghassemi, and F. Mirzaie, "Changes in *in vivo* confocal microscopic findings of ocular surface squamous neoplasia during treatment with topical interferon alfa-2b," *Ocular Surf.*, vol. 16, no. 2, pp. 235–241, 2018.

[17] L. M. Vajzovic, C. L. Karp, P. Haft, M. A. Shousha, S. R. Dubovy, V. Hurmeric, S. H. Yoo, and J. Wang, "Ultra high-resolution anterior segment optical coherence tomography in the evaluation of anterior corneal dystrophies and degenerations," *Ophthalmology*, vol. 118, no. 7, pp. 1291–1296, 2011.

[18] A. A. Nanji, C. Mercado, A. Galor, S. Dubovy, and C. L. Karp, "Updates in ocular surface tumor diagnostics," *Ophthalmology*, vol. 57, no. 3, pp. 47–62, 2017.

[19] M. Gosnel, "Unlocking the potential of spectral imaging for the characterization of cells and stem cells population," M.S. thesis, Macquarei Univ., North Ryde, NSW, Australia. 2013.

[20] M. G. V. Heiden, L. C. Cantley, and C. B. Thompson, "Understanding the Warburg effect: The metabolic requirements of cell proliferation," *Science*, vol. 324, no. 5930, pp. 1029–1033, 2009.

[21] B.-H. Li and S.-S. Xie, "Autofluorescence excitation-emission matrices for diagnosis of colonic cancer," *World J. Gastroenterol.*, vol. 11, no. 25, pp. 3931–3934, 2005.

[22] K. Moesta, B. Ebert, T. Handke, D. Nolte, C. Nowak, W. E. Haensch, R. K. Pandey, T. J. Dougherty, H. Rinneberg, and P. M. Schlag "Protoporphyrin IX occurs naturally in colorectal cancers and their metastases," *Cancer Res.*, vol. 61, no. 3, pp. 991–999, 2001.

[23] G. A. Wagnieres, W. M. Star, and B. C. Wilson, "*In Vivo* fluorescence spectroscopy and imaging for oncological applications," *Photochem. Photobiol.*, vol. 68, no. 5, pp. 603–632, 1998.

[24] M. Yung, M. A. Klufas, and D. Sarraf, "Clinical applications of fundus autofluorescence in retinal disease," *Int. J. Retina Vitreous*, vol. 2, no. 1, p. 12, 2016.

[25] A. Ly, L. Nivison-Smith, N. Assaad, and M. Kalloniatis, "Multispectral pattern recognition reveals a diversity of clinical signs in intermediate age-related macular degeneration," *Investigative Ophthalmol. Vis. Sci.*, vol. 59, no. 5, pp. 1790–1799, 2018.

[26] A. M. Poothullil and K. A. Colby, "Topical medical therapies for ocular surface tumors," *Seminars Ophthalmol.*, vol. 21, no. 3, pp. 161–169, 2006.

[27] S. Imada, "Camera and camera system capable of changing gain value and exposure time," U.S. Patent 7 414 648 B2, Feb. 19, 2008.

[28] A. R. Bentivoglio, S. B. Bressman, E. Cassetta, D. Carretta, P. Tonali, and A. Albanese, "Analysis of blink rate patterns in normal subjects," *Movement Disorders*, vol. 12, no. 6, pp. 1028–1034, 1997.

[29] R. Mayeux, "Biomarkers: Potential uses and limitations," *NeuroRx*, vol. 1, no. 2, pp. 182–188, 2004.

[30] Q. Du and H. Yang, "Similarity-based unsupervised band selection for hyperspectral image analysis," *IEEE Geosci. Remote Sens. Lett.*, vol. 5, no. 4, pp. 564–568, Oct. 2008.

[31] B. Wu, C. Chen, T. M. Kechadi, and L. Sun, "A comparative evaluation of filter-based feature selection methods for hyper-spectral band selection," *Int. J. Remote Sens.*, vol. 34, no. 22, pp. 7974–7990, 2013.

[32] C. Ding and H. Peng, "Minimum redundancy feature selection from microarray gene expression data," *J. Bio. Comput. Biol.*, vol. 3, no. 2, pp. 185–205, 2005.

[33] I. Guyon and A. Elisseeff, "An introduction to variable and feature selection," *J. Mach. Learn. Res.*, vol. 3, pp. 1157–1182, Mar. 2003.

[34] G. Lu and B. Fei, "Medical hyperspectral imaging: A review," *J. Biomed. Opt.*, vol. 19, no. 1, 2014, Art. no. 010901.

[35] J. Liu, S. Ranka, and T. Kahveci, "Classification and feature selection algorithms for multi-class CGH data," *Bioinformatics*, vol. 24, no. 13, pp. i86–i95, 2008.

[36] M. E. Gosnell, A. G. Anwer, J. C. Cassano, C. M. Sue, and E. M. Goldys, "Biochimica et Biophysica Acta (BBA) - Molecular Cell Research Functional hyperspectral imaging captures subtle details of cell metabolism in olfactory neurosphere cells, disease-specific models of neurodegenerative disorders," *Biochimica et Biophys. Acta (BBA) Mol. Cell Res.*, vol. 1863, no. 1, pp. 56–63, 2016.

[37] H. W. Ressom, R. S. Varghese, S. K. Drake, G. L. Hortin, M. Abdel-Hamid, C. A. Loffredo, and R. Goldman, "Peak selection from MALDI-TOF mass spectra using ant colony optimization," *Bioinformatics*, vol. 23, no. 5, pp. 619–626, 2007.

[38] S. Garnier, J. Gautrais, and G. Theraulaz, "The biological principles of swarm intelligence," *Swarm Intell.*, vol. 1, no. 1, pp. 3–31, 2007.

[39] C. Blum and X. Li, "Swarm intelligence in optimization," in *Swarm Intelligence*. Berlin, Germany: Springer, 2008, pp. 43–85.

[40] G. Beni, "Swarm intelligence," in *Encyclopedia of Complexity and Systems Science*. New York, NY, USA: Springer, 2009, pp. 1–32.

[41] B. K. Panigrahi and Y. M.-H. Shi Lim, *Handbook of Swarm Intelligence: Concepts, Principles and Applications*, Vol. 8. Berlin, Germany: Springer, 2011.

[42] X. Hu, Y. Shi, and R. Eberhart, "Recent advances in particle swarm," in *Proc. Congr. Evol. Comput.*, Jun. 2004, pp. 90–97.

[43] Martin E. Gosnell, A. G. Anwer, S. B. Mahbub, S. M. Perinchery, D. W. Inglis, P. P. Adhikary, J. A. Jazayeri, M. A. Cahill, S. Saad, C. A. Pollock, M. L. Sutton-McDowall, J. G. Thompson, and E. M. Goldys, "Quantitative non-invasive cell characterisation and discrimination based on multispectral autofluorescence features," *Sci. Rep.*, vol. 6, p. 23453, Mar. 2016.

[44] V. Vapnik, *The Nature of Statistical Learning Theory*. New York, NY, USA: Springer, 2013.

[45] T. S. Furey, N. Cristianini, N. Duffy, D. W. Bednarski, M. Schummer, and D. Haussler, "Support vector machine classification and validation of cancer tissue samples using microarray expression data," *Bioinformatics*, vol. 16, no. 10, pp. 906–914, 2000.

[46] Y.-W. Chen and C.-J. Lin, "Combining SVMs with various feature selection strategies," in *Feature extraction*. Berlin, Germany: Springer, 2006, pp. 315–324.
[47] T. Fawcett, "An introduction to ROC analysis," *Pattern Recognit. Lett.*, vol. 27, no. 8, pp. 861–874, Jun. 2006.
[48] A. Habibalahi and M. S. Safizadeh, "Pulsed eddy current and ultrasonic data fusion applied to stress measurement," *Meas. Sci. Technol.*, vol. 25, no. 5, 2014, Art. no. 055601.
[49] D. P. Mandic, D. Obradovic, A. Kuh, T. Adali, U. Trutschell, M. Golz, P. De Wilde, J. Barria, A. Constantinides, and J. Chambers, "Data fusion for modern engineering applications: An overview,"in *Proc. Int. Conf. Artif. Neural Netw.* Springer, 2005, pp. 715–721.
[50] S. Basti and M. S. Macsai, "Ocular surface squamous neoplasia: A review," *Cornea*, vol. 22, no. 7, pp. 687–704, 2003.
[51] Y. J. Kim, J. Kim, H. Choung, M. K. Kim, and W. R. Wee, "Conjunctival granuloma with necrosis associated with exposed suture in upper double lid masquerading as ocular surface squamous neoplasia: A case report," *BMC ophthalmol.*, vol. 17, no. 1, p. 55, 2017.
[52] S. B. Mahbub, M. Plöschner, M. E. Gosnell, A. G. Anwer, and E. M. Goldys, "Statistically strong label-free quantitative identification of native fluorophores in a biological sample," *Sci. Rep.*, vol. 7, no. 1, p. 15792, 2017.
[53] S. Arlot and A. Celisse, "A survey of cross-validation procedures for model selection," *Statist. Surv.*, vol. 4, no. 4, pp. 40–79, 2010.
[54] P. Refaeilzadeh and L. Liu, "Cross-validation," in *Encyclopedia of Database Systems*. Springer, 2009, pp. 532–538.
[55] F. De la Torre and T. Kanade, "Discriminative cluster analysis," in *Proc. 23rd Int. Conf. Mach. Learn.*, 2006, pp. 241–248.
[56] K. Tsuda, M. Kawanabe, and K.-R. Müller, "Clustering with the Fisher score,"in *Proc. Adv. Neural Inf. Process. Syst.*, 2003, pp. 745–752.
[57] J. Kennedy, "Swarm intelligence," in *Handbook of Nature-Inspired and Innovative Computing*. Boston, MA, USA: Springer, 2006, pp. 187–219.
[58] M. Dorigo and M. Birattari, "Ant colony optimization," in *Encyclopedia of Machine Learning*. New York, NY, USA: Springer, 2011, pp. 36–39.
[59] M. Shamsipur, V. Zare-Shahabadi, B. Hemmateenejad, and M. Akhond, "Ant colony optimisation: A powerful tool for wavelength selection," *J. Chemometrics*, vol. 20, nos. 3–4, pp. 146–157, 2006.
[60] A. P. Engelbrecht, *Fundamentals of Computational Swarm Intelligence*. Hoboken, NJ, USA: Wiley, 2006.
[61] R. Poli, J. Kennedy, and T. Blackwell, "Particle swarm optimization," *Swarm Intell.*, vol. 1, no. 1, pp. 33–57, Jun. 2007.
[62] R. C. Eberhart and Y. Shi, "Particle swarm optimization: Developments, applications and resources," in *Proc. Congr. Evol. Comput.*, May 2001, pp. 81–86.
[63] C. Zhang, J. Ning, S. Lu, D. Ouyang, and T. Ding, "A novel hybrid differential evolution and particle swarm optimization algorithm for unconstrained optimization," *Oper. Res. Lett.*, vol. 37, no. 2, pp. 117–122, 2009.
[64] K. Deb, "Multi-objective optimization," in *Search Methodologies: Introductory Tutorials in Optimization and Decision Support Techniques*. Boston, MA, USA: Springer, 2014, pp. 403–449.
[65] P. Cunningham and S. J. Delany, "K-Nearest neighbour classifiers," *Multiple Classifier Syst.*, vol. 34, pp. 1–17, Mar. 2007.